Journal of Hydrology 405 (2011) 488–500

Contents lists available at ScienceDirect

Journal of Hydrology

journal homepage: www.elsevier.com/locate/jhydrol

# A drawdown solution for constant-flux pumping in a confined anticline aquifer

Yen-Ju Chen [a], Hund-Der Yeh [a,*], Chia-Chen Kuo [b]

[a] Institute of Environmental Engineering, National Chiao Tung University, 1001 University Road, Hsinchu 300, Taiwan
[b] National Center for High-Performance Computing, National Applied Research Laboratories, Hsinchu 300, Taiwan

ARTICLE INFO

*Article history:*
Received 26 October 2010
Received in revised form 15 April 2011
Accepted 29 May 2011
Available online 12 June 2011
This manuscript was handled by P. Baveye, Editor-in-Chief, with the assistance of Renduo Zhang, Associate Editor

*Keywords:*
Anticline aquifer
Pumping test
Partially penetrating well
Anisotropy
Integral transform

SUMMARY

An anticline, known as a convex-upward fold in layers of rock, commonly is formed during lateral compression, which may be elected as a potential site for carbon sequestration. A mathematical model is developed in this study for describing the steady-state drawdown distribution in an anticline aquifer in response to the constant-flux pumping. The topographical shape of the anticline is mimicked by three successive blocks. The solution is obtained by applying the infinite Fourier transform and the finite Fourier cosine transform in each blocks and acquiring the hydraulic continuities between the blocks. Simulated results reveal that the introduction of a thin-limbs or narrow-ridged anticline would produce a much greater head drop in the ridge zone. For a well of constant pumping rate, the dimensionless drawdown around the well increases with decreasing well screen length or/and aquifer anisotropy ratio. An examination of the effect of well location on the drawdown reveals that the partially penetrating well located at the top-middle of the ridge zone produces the largest drawdown. The simulation of the flow in an anticline aquifer based on MODFLOW results in slightly smaller drawdown values in most regions when compared with those predicted by the present solution. The present solution can also be used to simulate the flow in a slab-shaped aquifer or a hillslope aquifer. It can be applied to determine the aquifer parameters if coupled with an optimization scheme and to provide the basis for selecting a potential site for carbon sequestration in the future as well.



## 1. Introduction

An anticline, as a result of lateral compression in crustal deformation, is a convex-upward fold in layers of rock. A well-structured anticline formation may be chosen as a candidate site for carbon sequestration. The movement of groundwater may carry the contaminants; therefore, explicit information such as geological structure and hydrogeological data are necessary to assess the applicability of the potential storage sites or to predict the migration of the contaminant plume in the site. Ashjari and Raeisi (2006) indicated that the anticline structure of aquifers and the geometry of bedrocks primarily dominate the direction of regional groundwater flow in an inquiry into the groundwater flow in Zagros anticlines in Iran. In recent years, several articles (e.g., Förster et al., 2006; Bergmann et al., 2010) have been devoted to the $CO_2$SINK project at Ketzin site in Germany. The Ketzin site is situated in the eastern part of the Roskow–Ketzin double anticline and selected to inject $CO_2$ to investigate the in situ physical, chemical, and biological process for geological carbon sequestration. Recently, numerical or analytical solutions were developed to investigate the head responses in anticline reservoirs due to the well injection or pumping. Al-Mohannadi et al. (2007) used a finite-difference method to simulate the transient pressure responses to horizontal wells in anticline reservoirs and curved wells in slab reservoirs. Yeh and Kuo (2010) proposed a steady-state analytical solution for a constant-head injection at a fully penetrating well into a heterogeneous, anisotropic, and dome-like anticline reservoir.

In engineering practices, a constant-flux pumping test withdraws water at a constant flow rate from the test well during the test period and measures the drawdown responses in one or more observation wells in the vicinity. Generally, a drawdown solution is either incorporated with an optimization technique or applied to generate the type curves for aquifer test interpretation to determine the best-fit aquifer parameters from the observed drawdown data. The Theis equation (1935) is the most popular tool used to estimate the drawdown distribution or to determine the aquifer parameters in an inverse problem for a constant-flux pumping in a confined aquifer. It would however not be appropriate to use the well and aquifer assumptions inherent in developing these equations to describe the flow in an anticline aquifer.

The integral transform method is used widely to deal with the groundwater flow problems edged with peculiar boundaries. For example, Chan et al. (1976) used the finite Fourier transform to develop the transient and steady-state drawdown solutions for pumping in a rectangular aquifer. Chan et al. (1978) and Yeh and Chang (2006) applied the finite sine transform and Hankel

* Corresponding author. Tel.: +886 3 5731910; fax: +886 3 5725958.
*E-mail address:* hdyeh@mail.nctu.edu.tw (H.-D. Yeh).

0022-1694/$ - see front matter © 2011 Elsevier B.V. All rights reserved.
doi:10.1016/j.jhydrol.2011.05.051

**Notation**

$a_i$ distance from the origin to the outer boundary of zone $i$ in $x$-direction (L)
$A_n$ function of $x_D$ defined by Eq. (23)
$b_i$ height of zone $i$ (L)
$B_k$ function of $x_D$ defined by Eq. (27)
$C_{1m}$, $C_{2m}$, $C_{4m}$, $C_{6m}$, $C_{7m}$ functions of $x_D$ defined by Eqs. (41), (42), (44), (46), and (47), respectively
$C_{3n}$, $C_{5k}$, $C_{8m}$, $C_{9m}$ constants defined by Eqs. (43), (45), (A22), and (A23), respectively
$D_{00}$, $D_{0i}$, $D_{n0}$, $D_{ni}$ constants defined by Eqs. (A2), (A3), (A4), and (A5), respectively
$E_{00}$, $E_{0j}$, $E_{n0}$, $E_{nj}$ constants defined by Eqs. (A6), (A7), (A8), and (A9), respectively
$F_{00}$, $F_{0i}$, $F_{k0}$, $F_{ki}$ constants defined by Eqs. (A10), (A11), (A12), and (A13), respectively
$G_{00}$, $G_{0j}$, $G_{k0}$, $G_{kj}$ constants defined by Eqs. (A14), (A15), (A16), and (A17), respectively
$k_x$, $k_y$, $k_z$ hydraulic conductivities in the $x$, $y$ and $z$ directions, respectively (L/T)
$l$ screen length (L)
$q$ volumetric pumping rate per unit length of the pumping well ($L^2$/T)
$q_D$ dimensionless volumetric pumping rate per unit length of the pumping well
$Q_D$ dimensionless volumetric pumping rate of the pumping well
$r_D$ dimensionless radial distance from the pumping well to the observation well
$RD$ relative difference calculated by Eq. (58)
$s_i$ drawdown in zone $i$ (L)
$s_{Di}$ dimensionless drawdown in zone $i$
$\bar{s}_{Di}$ dimensionless drawdown for zone $i$ in Fourier domain
$\hat{\bar{s}}_{D1P}, \hat{\bar{s}}_{D1N}$ dimensionless drawdown for zones 1P and 1N in Fourier and finite Fourier cosine domain, respectively
$S$ storativity of the aquifer
$S_0$, $S_n$ constants defined by Eqs. (A18) and (A19)
$t_D$ dimensionless time defined by Eq. (57)
$T$ transmissivity of the aquifer ($L^2$/T)
$T_0$, $T_k$ constants defined by Eqs. (A20) and (A21)
$u_p$, $u_{im}$, $u_{in}$ dimensionless variables in well functions, defined by Eqs. (54), (55), and (56), respectively
$U$ unit step function
$U_c$, $U_{c0}$, $U_{cm}$ constants defined by Eq. (32)
$V_0$, $V_n$ coefficients in Eqs. (22), (38), and (39)
$W_0$, $W_k$ coefficients in Eqs. (26), (38), and (39)
$W$ well function
$x_0$, $y_0$, $z_0$ coordinate of the top point of the pumping well
$x_{0D}$, $y_{0D}$, $z_{0D}$ dimensionless coordinate of the top point of the pumping well
$x_D$, $y_D$, $z_D$ dimensionless coordinate variables
$x_{Dai}$ dimensionless $x$-direction distance from the origin to the outer boundary of zone $i$
$z_{Dbi}$ dimensionless height of zone $i$
$z_{Dl}$ dimensionless screen length of the pumping well
$\alpha_n$ constant defined by Eq. (24)
$\beta_k$ constant defined by Eq. (28)
$\chi_{yx}$, $\chi_{zx}$ anisotropy ratios
$\delta$ Dirac delta function
$\varepsilon$ Fourier transform variable
$\phi(m, n)$ constant defined by Eq. (48)
$\gamma_m$ constant defined by Eq. (40)
$\lambda_m$ finite Fourier cosine transform variable used with respect to Eq. (1) and defined by Eq. (31)
$\theta$ angle between the positive $x_D$-axis and the line connecting the pumping and observation well
$\vartheta(m, k)$ constant defined by Eq. (49)
$\omega_n$ finite Fourier cosine transform variable used with respect to Eq. (10) and defined by Eq. (25)
$\zeta_k$ finite Fourier cosine transform variable used with respect to Eq. (16) and defined by Eq. (29)

transform to develop the transient and steady-state analytical solutions for head distribution in a wedge-shaped aquifer. On the other hand, some drawdown solutions accounting for various topography boundaries in flow systems are developed based on the image-well method. The method removes aquifer boundaries and place pumping or recharging image wells at judicious locations. The drawdown in an observation well is calculated by summing up the drawdown or buildup due to the real well and image wells (Ferris et al., 1962; Streltsova, 1988; Chen et al., 2009).

The domain decomposition method (DDM) can be applied to handle the problem with complex geometry or mix-typed boundary by splitting the problem domain into several subdomains. The solutions for each subdomain are developed to satisfy the corresponding boundary conditions as well as the continuities of head and flux at the interface between the connected elements. The concept of DDM was first presented in Kirkham (1957) to calculate the electrostatic potential between two concentric coaxial capped cylinders. The procedure was further extended in Kirkham (1959) to develop the hydraulic head solution for the flow toward a partially penetrating well in a confined aquifer. Later, Javandel and Zaghi (1975) used a similar procedure to obtain the potential distribution in a confined aquifer due to the pumping at a well vertically and fully penetrating the aquifer and of radially finite extension on the bottom of the aquifer. A similar decomposition concept was also applied by Connell et al. (1998) for solving the problem of topographically driven flow in hillslope aquifers by dividing the problem domain into several rectangular elements.

The objective of this study is to develop a mathematical model for describing the steady-state drawdown distribution in response to a constant-flux pumping in an anticline aquifer. A pumping well of infinitesimal diameter partially or fully penetrates the aquifer. The anticline aquifer is homogeneous, anisotropic and confined by a curved layer on the top and a horizontal impermeable layer at the bottom. Based on the DDM, the solution of the model is obtained by applying the integral transform techniques including Fourier transform (FT) and finite Fourier cosine transform (FFCT) within each block. The solution is useful in predicting the spatial drawdown distribution in a wide variety of anticline aquifer systems and investigating the influences of well location, screen length, aquifer geometry and anisotropy on the groundwater flow system. Moreover, the present solution may be applied to simulate the flow in hillslope and slab-shaped aquifers by assuming some of the adjacent blocks with the same heights. In addition to the analytical approach, the numerical model, MODFLOW, is used to perform simulations and the results are compared with those predicted by the present solution. The present solution can serve as an invaluable tool for gaining physical insight of the behavior of groundwater flow affected by geologic and geometric settings and for determining the aquifer parameters in an inverse problem if integrated with an optimization algorithm.

## 2. Methodology

### 2.1. Mathematical modeling of the flow problem

Fig. 1 sketches the configuration for a well in an anticline aquifer. Assume that the line sink, i.e., the pumping well of an infinitesimal radius, is extended along the $z$ direction with length $l$ from the point $(x_0, y_0, z_0) = (0, 0, z_0)$. The anticline aquifer is of a finite width in the $x$ direction, a finite thickness in the $z$ direction, but infinite extent in both $\pm y$ directions. In addition, the aquifer is confined, homogeneous, and anisotropic with the hydraulic conductivities of $k_x$, $k_y$ and $k_z$ in the $x$, $y$ and $z$ directions, respectively. To simplify the flow problem, three successive blocks with different heights and widths are used to mimic the topographical shape of anticline aquifer. The height of the middle block is determined by the acme of the anticline structure, while those of the adjacent blocks are designated by the corresponding margins of the limbs. The adopted widths of the blocks should make the simulated aquifer have the same volume as the original one as possible. Furthermore, the anticline aquifer is decomposed into four subdomains, i.e., zones 1P, 1N, 2 and 3, according to the shapes of blocks and the well location.

The mathematical model is developed in a dimensionless form to produce the simulated results in the most general way. The height of the middle block, $b_1$, is chosen as a reference length to nondimensionalize other variables. The dimensionless variables and parameters are defined as follows: $x_D = x/b_1$, $y_D = y/b_1$, and $z_D = z/b_1$ denoting the dimensionless coordinate variables; $x_{0D} = x_0/b_1$, $y_{0D} = y_0/b_1$, and $z_{0D} = z_0/b_1$ representing the top point of the pumping well in the dimensionless form; $x_{Dai} = a_i/b_1$ representing the dimensionless distance in $x$-direction of the outer boundary from the origin in zone $i$; $z_{Dbi} = b_i/b_1$ defining the dimensionless height of zone $i$, except that $z_{Db1} = 1$ standing for those in zones 1P and 1N; $s_{Di} = s_i/b_1$ denoting the dimensionless drawdown in zone $i$, where the notation $s_i$ is the drawdown in zone $i$ (L); $z_{Dl} = l/b_1$ representing the dimensionless screen length of the pumping well; $q_D = q/k_x b_1$ expressing the dimensionless volumetric pumping rate per unit length of the pumping well, where the notation $q$ is the volumetric pumping rate per unit length ($L^2\,T^{-1}$); $\chi_{yx} = k_y/k_x$ and $\chi_{zx} = k_z/k_x$ representing the anisotropy ratios.

#### 2.1.1. Formulation for flow in zone 1

In the development of the mathematical model, the middle block (shown in Fig. 1) is regarded as zone 1, which includes zones 1P and 1N. The steady-state groundwater flow to the pumping well in zone 1 is governed by

$$\frac{\partial^2 s_{D1}}{\partial x_D^2} + \chi_{yx}\frac{\partial^2 s_{D1}}{\partial y_D^2} + \chi_{zx}\frac{\partial^2 s_{D1}}{\partial z_D^2} = -q_D\{U[z_D - (z_{0D} - z_{Dl})] - U(z_D - z_{0D})\}\delta(x_D - x_{0D})\delta(y_D - y_{0D}), \quad x_{Da1N} \leqslant x_D \leqslant x_{Da1P}, \quad -\infty \leqslant y_D \leqslant \infty, \quad 0 \leqslant z_D \leqslant 1 \tag{1}$$

where $U$ and $\delta$ are the unit step function and Dirac delta function, respectively. The sink term in Eq. (1) implies that the flux through the screen is of uniform strength. The boundary conditions at infinity from the sink in the $y$ direction are assumed to be

$$s_{D1}(x_D, \pm\infty, z_D) = 0 \tag{2}$$

and

$$\frac{\partial s_{D1}(x_D, \pm\infty, z_D)}{\partial y_D} = 0 \tag{3}$$

For a confined aquifer, the conditions at the top and bottom impermeable boundaries are respectively written as

$$\frac{\partial s_{D1}(x_D, y_D, 1)}{\partial z_D} = 0 \tag{4}$$

and

$$\frac{\partial s_{D1}(x_D, y_D, 0)}{\partial z_D} = 0 \tag{5}$$

The continuities of flux and drawdown at the right-hand edge of zone 1 are respectively given as

$$\frac{\partial s_{D1}(x_{Da1P}, y_D, z_D)}{\partial x_D} = \frac{\partial s_{D2}(x_{Da1P}, y_D, z_D)}{\partial x_D}, \quad 0 \leqslant z_D < z_{Db2} \tag{6a}$$

$$\frac{\partial s_{D1}(x_{Da1P}, y_D, z_D)}{\partial x_D} = 0, \quad z_{Db2} \leqslant z_D \leqslant 1 \tag{6b}$$

and

$$s_{D1}(x_{Da1P}, y_D, z_D) = s_{D2}(x_{Da1P}, y_D, z_D), \quad 0 \leqslant z_D < z_{Db2} \tag{7}$$

Similarly, for the left-hand edge of zone 1, the following conditions should be satisfied:

$$\frac{\partial s_{D1}(x_{Da1N}, y_D, z_D)}{\partial x_D} = \frac{\partial s_{D3}(x_{Da1N}, y_D, z_D)}{\partial x_D}, \quad 0 \leqslant z_D < z_{Db3} \tag{8a}$$

$$\frac{\partial s_{D1}(x_{Da1N}, y_D, z_D)}{\partial x_D} = 0, \quad z_{Db3} \leqslant z_D \leqslant 1 \tag{8b}$$

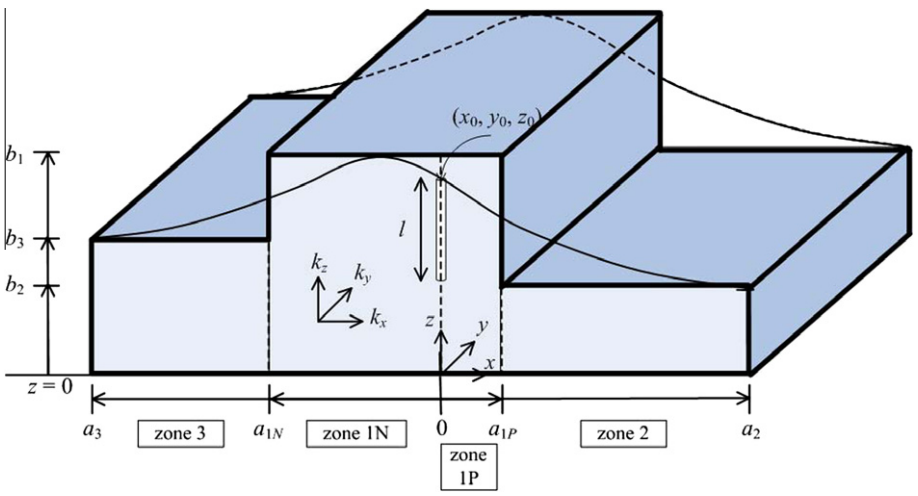


**Fig. 1.** Schematic representation of a groundwater flow problem in an anticline aquifer with a line sink located along the $z$ axis. The anticline aquifer is approximately divided into three blocks.

and

$$s_{D1}(x_{Da1N}, y_D, z_D) = s_{D3}(x_{Da1N}, y_D, z_D), \quad 0 \leqslant z_D < z_{Db3} \tag{9}$$

*2.1.2. Formulation for flow in zone 2*

The steady-state groundwater flow equation in zone 2 is expressed as:

$$\frac{\partial^2 s_{D2}}{\partial x_D^2} + \chi_{yx}\frac{\partial^2 s_{D2}}{\partial y_D^2} + \chi_{zx}\frac{\partial^2 s_{D2}}{\partial z_D^2} = 0, \quad x_{Da1P} \leqslant x_D \leqslant x_{Da2}, \quad -\infty \leqslant y_D \leqslant \infty, \quad 0 \leqslant z_D \leqslant z_{Db2} \tag{10}$$

The boundary conditions at infinity in the ±*y* directions require that

$$s_{D2}(x_D, \pm\infty, z_D) = 0 \tag{11}$$

and

$$\frac{\partial s_{D2}(x_D, \pm\infty, z_D)}{\partial y_D} = 0 \tag{12}$$

The no-flow conditions hold at the top and bottom boundaries respectively as

$$\frac{\partial s_{D2}(x_D, y_D, z_{Db2})}{\partial z_D} = 0 \tag{13}$$

and

$$\frac{\partial s_{D2}(x_D, y_D, 0)}{\partial z_D} = 0 \tag{14}$$

Assume a constant-head boundary located at the lateral distance of $x_{Da2}$ from the pumping well; that is,

$$s_{D2}(x_{Da2}, y_D, z_D) = 0 \tag{15}$$

Note that Eqs. (6a) and (7), representing the continuity conditions of flux and drawdown at the interface between zones 1P and 2, are the left-hand boundary conditions of zone 2.

*2.1.3. Formulation for flow in zone 3*

The steady-state groundwater flow equation in zone 3 is given by

$$\frac{\partial^2 s_{D3}}{\partial x_D^2} + \chi_{yx}\frac{\partial^2 s_{D3}}{\partial y_D^2} + \chi_{zx}\frac{\partial^2 s_{D3}}{\partial z_D^2} = 0, \quad x_{Da3} \leqslant x_D \leqslant x_{Da1N}, \quad -\infty \leqslant y_D \leqslant \infty, \quad 0 \leqslant z_D \leqslant z_{Db3} \tag{16}$$

The boundary conditions at infinite distance in the ± *y* directions require that

$$s_{D3}(x_D, \pm\infty, z_D) = 0 \tag{17}$$

and

$$\frac{\partial s_{D3}(x_D, \pm\infty, z_D)}{\partial y_D} = 0 \tag{18}$$

The top and bottom conditions in zone 3 are respectively given as

$$\frac{\partial s_{D3}(x_D, y_D, z_{Db3})}{\partial z_D} = 0 \tag{19}$$

and

$$\frac{\partial s_{D3}(x_D, y_D, 0)}{\partial z_D} = 0 \tag{20}$$

A constant-head condition is applied at the lateral distance of $x_{Da3}$ from the pumping well, which is described as

$$s_{D3}(x_{Da3}, y_D, z_D) = 0 \tag{21}$$

Furthermore, Eqs. (8a) and (9) state the continuity requirements of flux and drawdown at the interface between zones 1N and 3.

*2.2. Analytical solutions*

*2.2.1. Dimensionless drawdown solutions in Fourier domain for zones 2 and 3*

To solve the partial differential Eqs. (1), (10), and (16) with their corresponding boundary conditions, the techniques of FT and FFCT are applied to the variables $y_D$ and $z_D$, respectively, to obtain the ordinary differential equations (ODEs) in terms of $x_D$. Note that formulas of FFCT applied to Eqs. (1), (10), and (16) are different since the independent variable $z_D$ ranges over different intervals in zones 1, 2, and 3, respectively. We first deal with the flow problem in zones 2 and 3 since their governing equations are simple and of the same form. The dimensionless drawdown solution of zone 2 in Fourier domain satisfying the conditions (10)–(15) is given as:

$$\bar{s}_{D2}(x_D, z_D) = V_0 A_0(x_D) + \sum_{n=1}^{\infty} V_n A_n(x_D)\cos(\omega_n z_D) \tag{22}$$

where

$$A_n(x_D) = \frac{\sinh[\alpha_n(x_{Da2} - x_D)]}{\sinh[\alpha_n(x_{Da2} - x_{Da1P})]}, \quad n = 0, 1, 2, 3, \ldots \tag{23}$$

with

$$\alpha_n = \sqrt{\varepsilon^2\chi_{yx} + \omega_n^2\chi_{zx}}, \quad n = 0, 1, 2, 3, \ldots \tag{24}$$

In Eq. (24), $\varepsilon$ is the FT transform variable; $\omega_n$, which is the transform variable applied to Eq. (10) in the FFCT for the integral interval $[0, z_{Db2}]$, is defined as

$$\omega_n = \frac{n\pi}{z_{Db2}}, \quad n = 0, 1, 2, 3, \ldots \tag{25}$$

Note that the coefficients $V_0$ and $V_n$ are the constants needed to be determined by the remaining boundary conditions (6a) and (7).

As for zone 3, the dimensionless drawdown solution of Eq. (16) in Fourier domain satisfying conditions (17)–(21) is expressed in the series form as:

$$\bar{s}_{D3}(x_D, z_D) = W_0 B_0(x_D) + \sum_{k=1}^{\infty} W_k B_k(x_D)\cos(\zeta_k z_D) \tag{26}$$

where

$$B_k(x_D) = \frac{\sinh[\beta_k(x_{Da3} - x_D)]}{\sinh[\beta_k(x_{Da3} - x_{Da1N})]}, \quad k = 0, 1, 2, 3, \ldots \tag{27}$$

with

$$\beta_k = \sqrt{\varepsilon^2\chi_{yx} + \zeta_k^2\chi_{zx}}, \quad k = 0, 1, 2, 3, \ldots \tag{28}$$

and $\zeta_k$, the transform variable used in the FFCT to Eq. (16) for the integral interval $[0, z_{Db3}]$, defined as

$$\zeta_k = \frac{k\pi}{z_{Db3}}, \quad k = 0, 1, 2, 3, \ldots \tag{29}$$

The coefficients $W_0$ and $W_k$ in Eq. (26) are the remaining undetermined constants.

*2.2.2. Dimensionless drawdown solution in Fourier domain for zone 1*

The FT with respect to $y_D$ and FFCT with respect to $z_D$ are applied to Eq. (1) and the result is

$$\frac{d^2\hat{\bar{s}}_{D1}}{dx_D^2} - (\varepsilon^2\chi_{yx} + \lambda_m^2\chi_{zx})\hat{\bar{s}}_{D1} = -q_D U_c \delta(x_D - x_{0D}), \quad x_{Da1N} \leqslant x_D \leqslant x_{Da1P} \tag{30}$$

where $\hat{\bar{s}}_{D1}$ is the dimensionless drawdown in Fourier and finite Fourier cosine domain; $\lambda_m$ is the transform variable used in the FFCT to Eq. (1) for the integral interval [0, 1], which is defined as

$$\lambda_m = m\pi, \quad m = 0, 1, 2, 3, \ldots \tag{31}$$

In addition,

$$U_c = \int_{z_{0D}-z_{Dl}}^{z_{0D}} \cos(\lambda_m z_D) dz_D \tag{32}$$

which can be reduced to $U_c = U_{c0} = z_{Dl}$ when $m = 0$; otherwise,

$$U_c = U_{cm} = \frac{\sin(\lambda_m z_{0D}) - \sin[\lambda_m(z_{0D} - z_{Dl})]}{\lambda_m}, \quad m = 1, 2, 3, \ldots \tag{33}$$

To solve Eq. (30) with the term of Dirac delta function, we consider the following sets of ODEs by dividing zone 1 into zones 1P and 1N as:

$$\frac{d^2\hat{\bar{s}}_{D1P}}{dx_D^2} - (\varepsilon^2\chi_{yx} + \lambda_m^2\chi_{zx})\hat{\bar{s}}_{D1P} = 0, \quad 0 < x_D \leqslant x_{Da1P} \tag{34}$$

and

$$\frac{d^2\hat{\bar{s}}_{D1N}}{dx_D^2} - (\varepsilon^2\chi_{yx} + \lambda_m^2\chi_{zx})\hat{\bar{s}}_{D1N} = 0, \quad x_{Da1N} \leqslant x_D < 0 \tag{35}$$

The boundary condition at $x_D = 0$ due to the continuity requirement, which is expressed as

$$\hat{\bar{s}}_{D1P}(0^+) = \hat{\bar{s}}_{D1N}(0^-) \tag{36}$$

Integration of Eq. (30) with respect to $x_D$ along $0^-$ to $0^+$ yields the second boundary condition as

$$\frac{d\hat{\bar{s}}_{D1P}(0^+)}{dx_D} - \frac{d\hat{\bar{s}}_{D1N}(0^-)}{dx_D} = -q_D U_c \tag{37}$$

The dimensionless drawdown solutions for zones 1P and 1N in Fourier domain can be obtained by taking the inversion of FFCT to the solutions of Eqs. (34) and (35) with conditions (36) and (37). Applying Eqs. (6) and (8) to the solutions of zones 1P and 1N, respectively, yields dimensionless drawdowns as

$$\bar{s}_{D1P}(x_D, z_D) = \frac{q_D U_{c0}}{2\gamma_0}[C_{10}(x_D) + C_{20}(x_D)] - z_{Db2}C_{30}C_{40}(x_D)V_0 + z_{Db3}C_{50}C_{60}(x_D)W_0 + \sum_{m=1}^{\infty}\left\{\begin{array}{l} \frac{q_D U_{cm}}{\gamma_m}[C_{1m}(x_D) + C_{2m}(x_D)] \\ -\frac{2}{\gamma_m}\left\{\left[\frac{\sin(\lambda_m z_{Db2})}{\lambda_m}\right]\alpha_0 C_{30}V_0 + \sum_{n=1}^{\infty}\phi(m,n)\alpha_n C_{3n}V_n\right\}C_{4m}(x_D) \\ +\frac{2}{\gamma_m}\left\{\left[\frac{\sin(\lambda_m z_{Db3})}{\lambda_m}\right]\beta_0 C_{50}W_0 + \sum_{k=1}^{\infty}\vartheta(m,k)\beta_k C_{5k}W_k\right\}C_{6m}(x_D) \end{array}\right\}\cos(\lambda_m z_D) \tag{38}$$

in zone 1P and

$$\bar{s}_{D1N}(x_D, z_D) = \frac{q_D U_{c0}}{2\gamma_0}[C_{10}(x_D) + C_{70}(x_D)] - z_{Db2}C_{30}C_{40}(x_D)V_0 + z_{Db3}C_{50}C_{60}(x_D)W_0 + \sum_{m=1}^{\infty}\left\{\begin{array}{l} \frac{q_D U_{cm}}{\gamma_m}[C_{1m}(x_D) + C_{7m}(x_D)] \\ -\frac{2}{\gamma_m}\left\{\left[\frac{\sin(\lambda_m z_{Db2})}{\lambda_m}\right]\alpha_0 C_{30}V_0 + \sum_{n=1}^{\infty}\phi(m,n)\alpha_n C_{3n}V_n\right\}C_{4m}(x_D) \\ +\frac{2}{\gamma_m}\left\{\left[\frac{\sin(\lambda_m z_{Db3})}{\lambda_m}\right]\beta_0 C_{50}W_0 + \sum_{k=1}^{\infty}\vartheta(m,k)\beta_k C_{5k}W_k\right\}C_{6m}(x_D) \end{array}\right\}\cos(\lambda_m z_D) \tag{39}$$

in zone 1N, where

$$\gamma_m = \sqrt{\varepsilon^2\chi_{yx} + \lambda_m^2\chi_{zx}}, \quad m = 0, 1, 2, 3, \ldots \tag{40}$$

$$C_{1m}(x_D) = \frac{\cosh[\gamma_m(x_{Da1P} + x_{Da1N} - x_D)]}{\sinh[\gamma_m(x_{Da1P} - x_{Da1N})]}, \quad m = 0, 1, 2, 3, \ldots \tag{41}$$

$$C_{2m}(x_D) = \frac{\cosh[\gamma_m(x_{Da1P} - x_{Da1N} - x_D)]}{\sinh[\gamma_m(x_{Da1P} - x_{Da1N})]}, \quad m = 0, 1, 2, 3, \ldots \tag{42}$$

$$C_{3n} = \coth[\alpha_n(x_{Da2} - x_{Da1P})], \quad n = 0, 1, 2, 3, \ldots \tag{43}$$

$$C_{4m}(x_D) = \frac{\cosh[\gamma_m(x_{Da1N} - x_D)]}{\sinh[\gamma_m(x_{Da1P} - x_{Da1N})]}, \quad m = 0, 1, 2, 3, \ldots \tag{44}$$

$$C_{5k} = \coth[\beta_k(x_{Da3} - x_{Da1N})], \quad k = 0, 1, 2, 3, \ldots \tag{45}$$

$$C_{6m}(x_D) = \frac{\cosh[\gamma_m(x_{Da1P} - x_D)]}{\sinh[\gamma_m(x_{Da1P} - x_{Da1N})]}, \quad m = 0, 1, 2, 3, \ldots \tag{46}$$

$$C_{7m}(x_D) = \frac{\cosh[\gamma_m(x_{Da1P} - x_{Da1N} + x_D)]}{\sinh[\gamma_m(x_{Da1P} - x_{Da1N})]}, \quad m = 0, 1, 2, 3, \ldots \tag{47}$$

$$\phi(m,n) = \begin{cases} \frac{\sin[(\lambda_m + \omega_n)z_{Db2}]}{2(\lambda_m + \omega_n)} + \frac{z_{Db2}}{2}, & \text{for } \lambda_m = \omega_n \quad (48a) \\ \frac{\sin[(\lambda_m + \omega_n)z_{Db2}]}{2(\lambda_m + \omega_n)} + \frac{\sin[(\lambda_m - \omega_n)z_{Db2}]}{2(\lambda_m - \omega_n)}, & \text{for } \lambda_m \neq \omega_n \quad (48b) \end{cases}$$

and

$$\vartheta(m,k) = \begin{cases} \frac{\sin[(\lambda_m + \zeta_k)z_{Db3}]}{2(\lambda_m + \zeta_k)} + \frac{z_{Db3}}{2}, & \text{for } \lambda_m = \zeta_k \quad (49a) \\ \frac{\sin[(\lambda_m + \zeta_k)z_{Db3}]}{2(\lambda_m + \zeta_k)} + \frac{\sin[(\lambda_m - \zeta_k)z_{Db3}]}{2(\lambda_m - \zeta_k)}, & \text{for } \lambda_m \neq \zeta_k \quad (49b) \end{cases}$$

Substituting Eqs. (22) and (38) into Eq. (7), the coefficients $V_0$ and $V_n$ can be expressed in terms of the functions of $V_0$, $V_n$, $W_0$ and $W_k$ via the determination of the coefficients in the Fourier cosine series. Similarly, the coefficients $W_0$ and $W_k$ are related to $V_0$, $V_n$, $W_0$ and $W_k$ by substituting Eqs. (26) and (39) into Eq. (9). The coefficients $V_0$, $V_n$, $W_0$ and $W_k$ can then be solved in the matrix form as presented in Appendix A (i.e., Eq. (A1)).

### 2.2.3. Inverse Fourier transform

The FT of function $f(y_D)$ with respect to the variable $y_D$ is defined as (Jeffrey and Dai, 2008):

$$\bar{f}(\varepsilon) = \int_{-\infty}^{\infty} f(y_D)e^{-i\varepsilon y_D} dy_D \tag{50}$$

where $\bar{f}(\varepsilon)$ is the transformed function and its inversion is expressed as

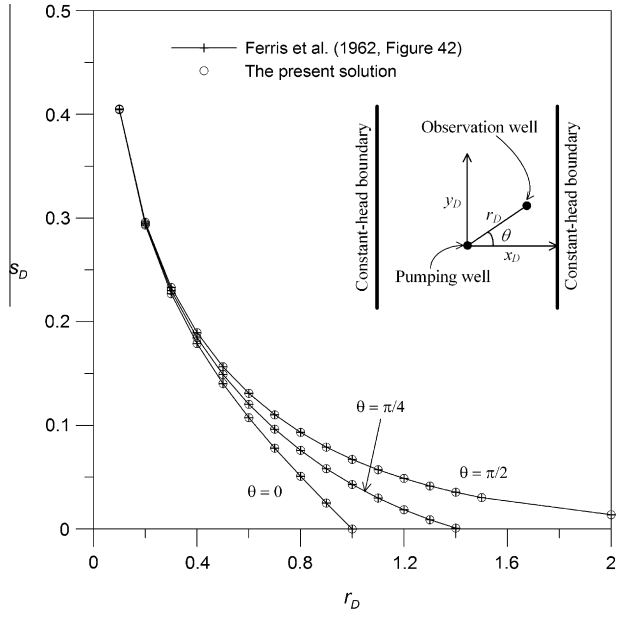


**Fig. 2.** The dimensionless drawdown distributions predicted by the present solution and the image-well method (Ferris et al., 1962) for pumping at the middle of a slab-shaped aquifer bounded by two parallel constant-head boundaries.

$$f(y_D) = \frac{1}{2\pi}\int_{-\infty}^{\infty} \bar{f}(\varepsilon) e^{i\varepsilon y_D} d\varepsilon \tag{51}$$

The function $\bar{f}(\varepsilon)$ refers to the drawdown solutions, Eqs. (22), (26), (38), and (39), in the Fourier domain for the flow in the anticline aquifer. Since the drawdown solutions are even functions with respect to the variable $\varepsilon$, Eq. (51) can be reduced to

$$f(y_D) = \frac{1}{\pi}\int_{0}^{\infty} \bar{f}(\varepsilon) \cos(\varepsilon y_D) d\varepsilon \tag{52}$$

The numerical calculation of Eq. (52) is achieved by the routine DQDAWF of IMSL (2003), which has the ability to cope with integrals of semi-infinite interval and of cosine or sine integrands.

## 3. Results and discussion

### 3.1. Special cases

#### 3.1.1. Slab-shaped aquifer bounded by parallel recharge boundaries

The present solution can be simplified to describe the pumping in an isotropic slab-shaped aquifer bounded by two parallel constant-head boundaries along $y$-direction if the three blocks are of the same height, i.e., $z_{Db1} = z_{Db2} = z_{Db3} = 1$. In this section, we assume a fully penetrating well pumped at a dimensionless flow rate of $Q_D = q_D z_{Dl} = 1$ and located at the middle of the slab-shaped aquifer with $x_{Da2} = 1$ and $x_{Da3} = -1$. The same problem refers to Ferris et al. (1962, Fig. 42), who illustrates the application of image-well method for the pumping in an aquifer bounded by two parallel boundaries. If an observation well is located at the dimensionless distance of $r_D$ from the pumping well, the dimensionless drawdown at the well can be formulated by superposition of Theis solution (1935) as

$$s_D(r_D, t_D) = \frac{Q_D}{4\pi}\left[W(u_p) + \sum_{m=1}^{\infty}(-1)^m W(u_{im}) + \sum_{n=1}^{\infty}(-1)^n W(u_{in})\right] \tag{53}$$

where $W$ is the well function; $u_p$, $u_{im}$, and $u_{in}$ are the dimensionless variables respectively defined as

$$u_p = \frac{r_D^2}{4t_D} \tag{54}$$

$$u_{im} = \frac{r_D^2 + 4m^2 - 4mr_D\cos\theta}{4t_D} \tag{55}$$

and

$$u_{in} = \frac{r_D^2 + 4n^2 - 4nr_D\cos(\pi-\theta)}{4t_D} \tag{56}$$

in which $\theta$ is the angle between the positive $x_D$-axis and the line connecting the pumping and observation wells; $t_D$ is the dimensionless time defined as

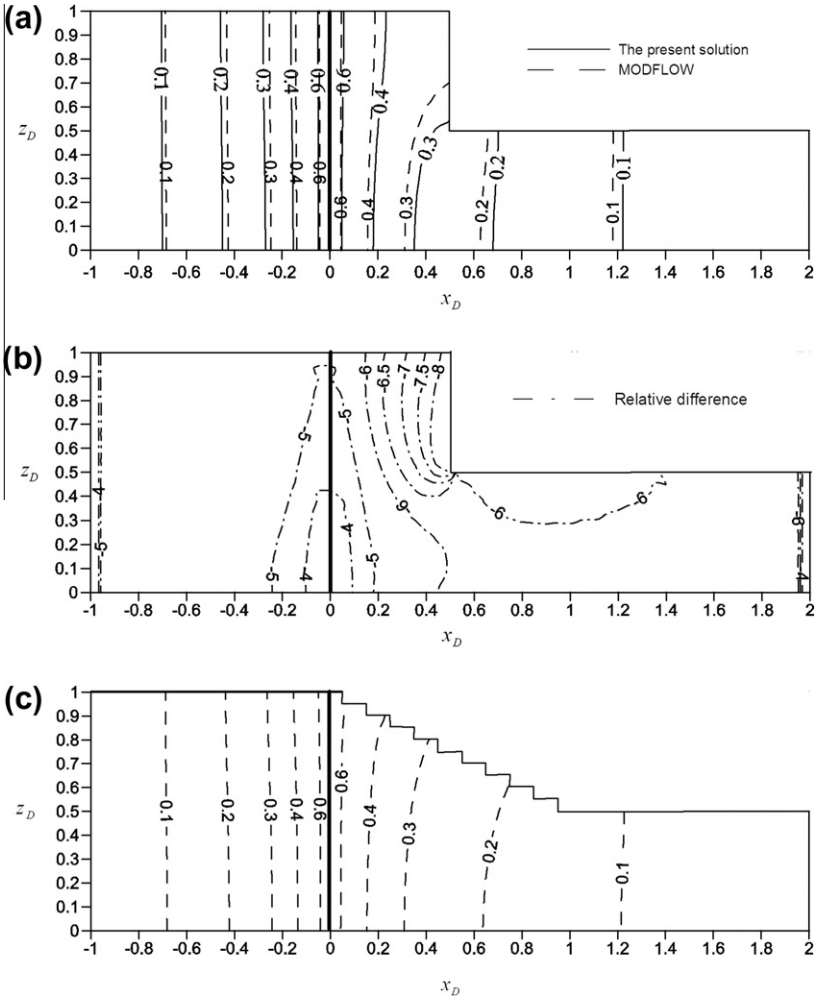


**Fig. 3.** Plots for the pumping at a fully penetrating well in a hillslope aquifer. The simulations were carried out by the present solution and MODFLOW for (a) dimensionless drawdown contours and (b) relative difference map in a step-like aquifer. In case (c), MODFLOW with multiple steps is used to approximate the inclined boundary.

$$t_D = \frac{Tt}{b_1^2 S} \tag{57}$$

with $T$ and $S$ representing the transmissivity and storativity of the aquifer, respectively. Note that when $t_D$ is large enough so that the flow system reaches the steady state, the dimensionless drawdowns calculated by the image-well method can then be compared to the simplified solution. Fig. 2 compares the dimensionless drawdown calculated by the present solution and Eq. (53) for pumping at the middle of the slab-shaped aquifer bounded by two parallel constant-head boundaries. The dimensionless drawdown are calculated along the radial direction for $\theta = 0$, $\pi/4$, and $\pi/2$. The dimensionless drawdown distributions predicted by the present solution in this special case match very well with those predicted by Eq. (53).

### 3.1.2. Hillslope aquifer

Fig. 3a shows the dimensionless drawdown distribution predicted by the present solution and MODFLOW for flow in a hillslope confined aquifer due to the pumping. The hillslope aquifer is mimicked by setting two of the adjacent blocks with the same height, which has the geometry of $x_{Da1P} = 0.5$, $x_{Da1N} = -0.5$, $x_{Da2} = 2$, $x_{Da3} = -1$, $z_{Db1} = z_{Db3} = 1$, and $z_{Db2} = 0.5$. In addition, a fully penetrating well pumped at a dimensionless pumping rate of $Q_D = 1$. In the simulation achieved by MODFLOW, the aquifer is assumed bounded by two parallel constant-head boundaries with the distance of 30 m in width. The aquifer thickness varies from 10 m to 5 m in the hillslope. Note that the infinite boundaries in the $\pm y$-directions are replaced by two assigned constant-head boundaries located at ±40 m from the pumping well. The hydraulic conductivities are $10^{-4}$ m/s in the $x$-, $y$- and $z$-directions. The pumping rate at the well is $10^{-2}$ m$^3$/s so that the dimensionless pumping rate will be $Q_D = 1$. The length of time is set to $9.46728 \times 10^7$ s (1095.75 day) for the steady-state simulation. The model domain has been discretized using a uniform cubic grid with a step of 0.5 m. That is, the aquifer is discretized with 21 layers, 61 columns, and 161 rows.

Fig. 3a shows that the dimensionless drawdown contours are influenced by the inclination in the hillslope aquifer. The vertical flow appears around the concave corner of the top boundary, while the flow seems horizontal elsewhere. The figure indicates that a slight difference in the drawdown distribution occurs near the concave corner of the top boundary between the present solution and MODFLOW. Fig. 3b is the relative difference map with the relative difference values calculated by

$$RD(\%) = \frac{s_{D,\mathrm{MODFLOW}} - s_{D,\mathrm{present\ solution}}}{s_{D,\mathrm{present\ solution}}} \times 100 \tag{58}$$

In Fig. 3b, the relative difference contours with negative values represent that the drawdown predicted by MODFLOW is smaller than that estimated by the present solution. The largest relative difference is up to 8% (absolute value) happening near the concave corner of the top boundary. Fig. 3c presents the simulated results from MODFLOW in a hillslope aquifer with more elaborate representation on the sloping boundary. The significant flexure contours between 0.2 and 0.6 reflect the influence of inclined top boundary on the flow pattern.

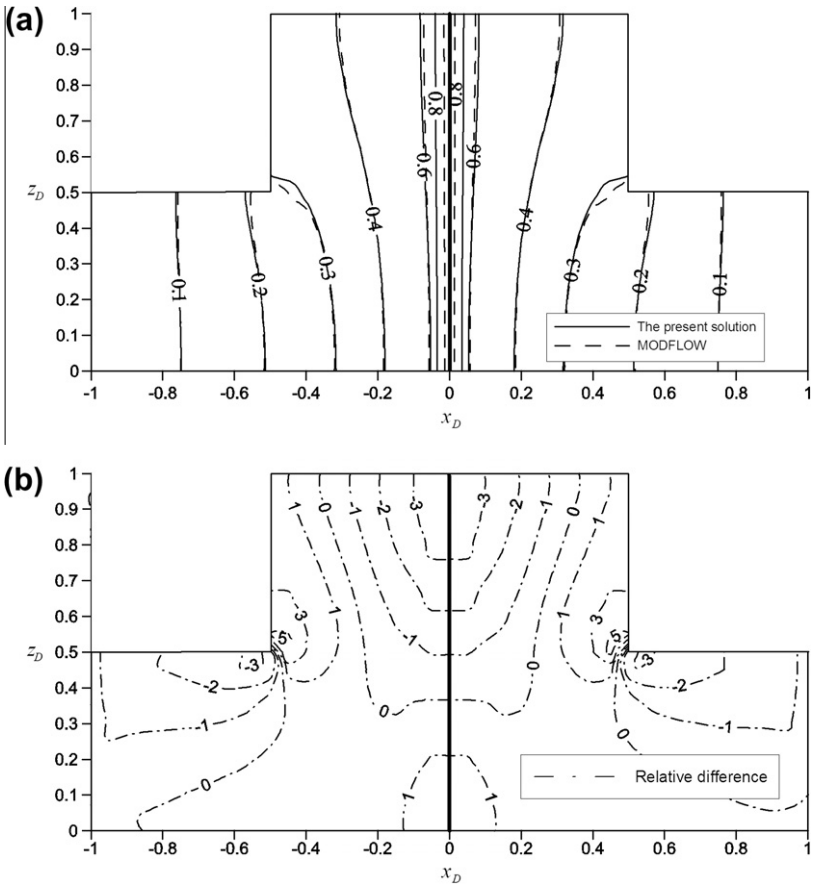


**Fig. 4.** (a) Dimensionless drawdown contours and (b) relative difference map on $x_D$–$z_D$ plane with $y_D = 0$ for pumping at a fully penetrating well in an isotropic and step-like anticline aquifer from the simulations carried out by the present solution and MODFLOW.

### 3.2. Effect of anticline aquifer geometry

#### 3.2.1. Base case of anticline aquifer

To investigate the influence of aquifer geometry on the flow pattern, we assume a simple case of a fully penetrating well located at an isotropic anticline aquifer. The aquifer geometry is characterized by $x_{Da1P} = 0.5$, $x_{Da1N} = -0.5$, $x_{Da2} = 1$, $x_{Da3} = -1$, and $z_{Db2} = z_{Db3} = 0.5$. The well pumps at a dimensionless flow rate of $Q_D = 1$. Fig. 4a depicts the dimensionless drawdown distribution in the $x_D$–$z_D$ plane for $y_D = 0$ predicted by the present solution and MODFLOW. In MODFLOW simulation, the anticline aquifer is bounded by two parallel constant-head boundaries with a distance of 20 m in width. The acme of the anticline structure is 10 m in height; the limbs intersect with the two parallel constant-head boundaries at 5 m in height. The settings of the $y$-direction boundaries, hydraulic conductivities, pumping rate and time length are the same as those used in the simulation of the hillslope aquifer flow. The aquifer is discretized into a mesh with 21 layers, 41 columns and 161 rows.

Fig. 4a reveals that most of water flows horizontally around the well screen and in the limbs; however, conspicuous vertical flow appears around the concave corner of the top boundary. The dimensionless drawdown contours intersect with the top and bottom impervious boundaries at right angles. The drawdown contours predicted by MODFLOW seem similar to those by the present solution except that slight differences can be observed near the concave corner of the top boundary and the pumping well. In Fig. 4b, the relative difference map clearly indicates that MODFLOW results in smaller dimensionless drawdown around the upper part of the pumping well and limb zones than the present solution. The drawdown predicted by MODFLOW is larger than that estimated by the present solution around the bottom part of the pumping well and near the concave corner of the top boundary. The largest relative difference is up to 5 % occurring near the concave corner of the top boundary.

Fig. 5a compares simulations of the dimensionless drawdown contours carried out by the present solution in a step-like aquifer (base case in Fig. 4a) and MODFLOW with multiple steps to approximate the inclined boundary. The MODFLOW settings of the $x$-direction and $y$-direction boundaries, hydraulic conductivities, pumping rate, time length, and grid discretization are the same as those used in the simulation of Fig. 4a. Fig. 5a shows the smooth and curved drawdown contours in the $y_D$–$z_D$ profile for $x_D = 0$. The contours intersected with the top boundaries at bevel angles due to the coarse discretization on the model grid. Fig. 5b shows the relative difference map of dimensionless drawdowns predicted by MODFLOW and the present solution on the overlapped region. The figure shows that MODFLOW gives smaller dimensionless drawdown than the present solution for the most part in the anticline and larger dimensionless drawdown at the upper parts of the limbs, when the simulation is achieved by approximating the top boundary of aquifer with multiple steps. The difference in the approximations of aquifer geometry would lead to the relative difference of the predicted dimensionless drawdowns between MODFLOW and the present solution up to 30% (absolute value). Overall, one may overestimate the dimensionless drawdown in most regions when applying the simple one-step like top boundary to simulate the anticlinal geometry.

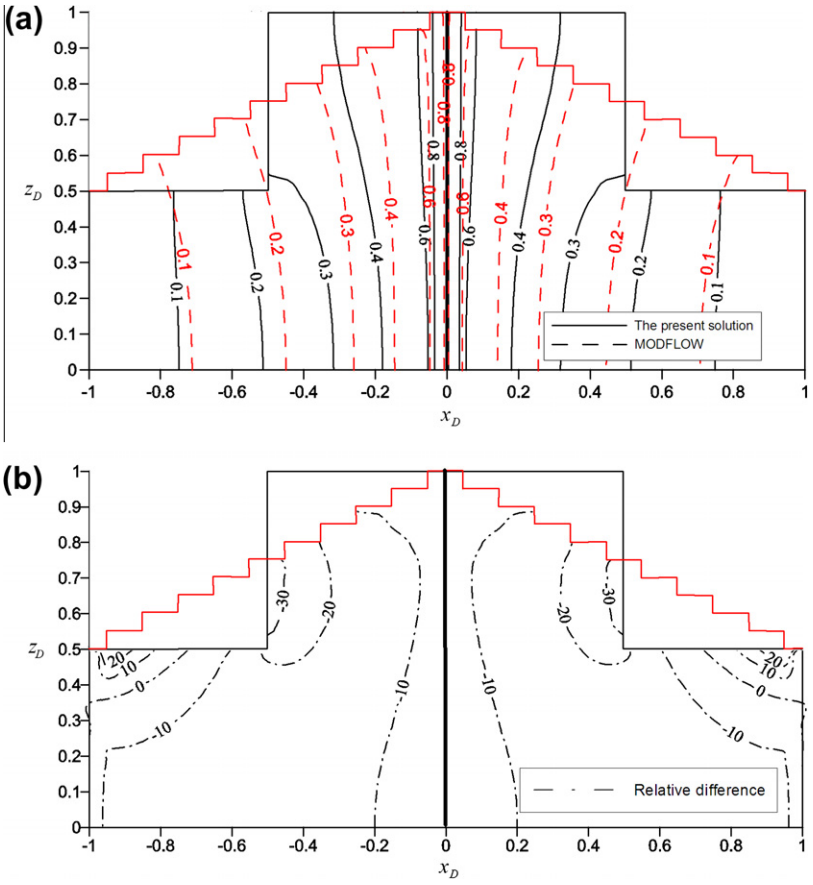


**Fig. 5.** (a) Dimensionless drawdown contours and (b) relative difference map on $x_D$–$z_D$ plane with $y_D = 0$ for pumping at a fully penetrating well in an isotropic anticline aquifer. The simulations were carried out by the present solution in a step-like aquifer and MODFLOW with multiple steps to approximate the inclined boundary.

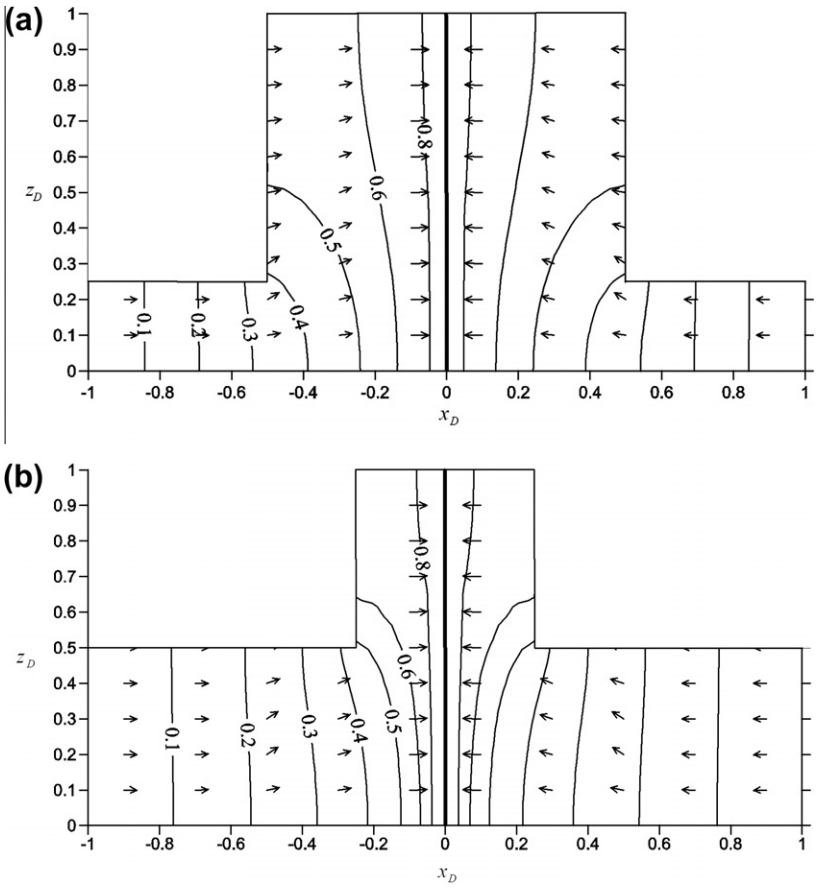


**Fig. 6.** Plots of dimensionless drawdown contours and flow fields for pumping at a fully penetrating well in an isotropic aquifer of (a) thin limbs and (b) narrow ridge.

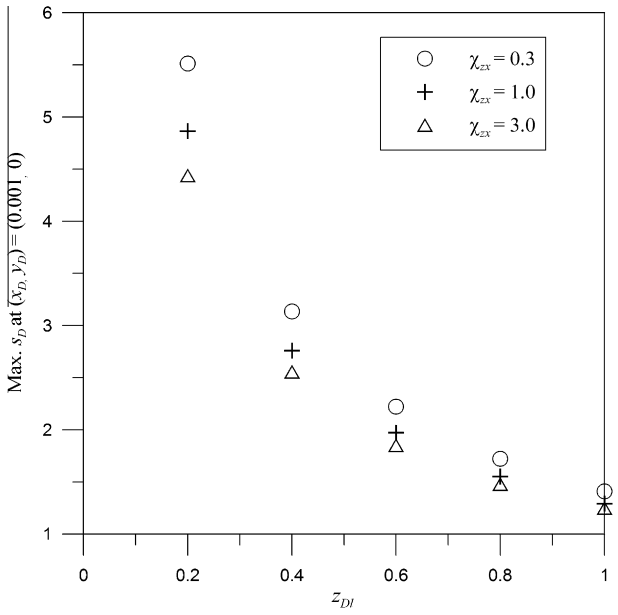


**Fig. 7.** A comparison of largest dimensionless drawdown at $(x_D, y_D) = (0.001, 0)$ for the cases of different screen lengths and aquifer anisotropy ratios. The wells are screened from the top-middle of the anticline aquifer. The geometry of the aquifer is the same as the base case shown in Fig. 4a.

### 3.2.2. Anticline aquifers of thin limbs and narrow ridge

Fig. 6 examines results obtained from flow in two other aquifers with different geometries by considering the aquifer portrayed in Fig. 4a as a base case. Fig. 6a illustrates the dimensionless drawdown contours for an anticline aquifer of thin limbs. The height of the limbs are reduced to half of that in the base case, i.e., $z_{Db2} = z_{Db3} = 0.25$. Fig. 6b depicts the case of narrow-ridged anticline with $x_{Da1P} = 0.25$ and $x_{Da1N} = -0.25$. Both figures show that most of water flows horizontally around the well and in the limbs. Significantly vertical flow appears around the concave corner of the top boundary in the ridge zone due to the geometric variation. In addition, the introduction of anticline aquifers with thin limbs or narrow ridge both produces a sharp head drop in the ridge zone in comparison with that of the base case at steady state.

## 3.3. Effect of well partial penetration

### 3.3.1. Effect of screen length and aquifer anisotropy

Fig. 7 demonstrates the largest dimensionless drawdown at $(x_D, y_D) = (0.001, 0)$ along the $z$-direction for the cases of different dimensionless screen length of $z_{Dl} = 0.2$, 0.4, 0.6, 0.8 and 1.0 and various aquifer anisotropy ratios of $\chi_{zx} = 0.3$, 1.0, and 3.0. The wells are screened from the top of the aquifer with a constant dimensionless pumping rate of $Q_D = 1$. Among these cases, the largest dimensionless drawdown appears at the case of the smallest $\chi_{zx}$ and $z_{Dl}$ ($\chi_{zx} = 0.3$ and $z_{Dl} = 0.2$) near the top of the aquifer. Moreover, the influence of aquifer anisotropy on the drawdown increases with the decrease of screen length.

Figs. 8a and b display the dimensionless drawdown contours for the anisotropic cases of $\chi_{zx} = 0.3$ and 3, respectively. In Fig. 8a, significant vertical flow can be observed in the ridge and limb zones. The contours for $s_D = 0.3$ to 0.8 are nearly horizontal, which reflect

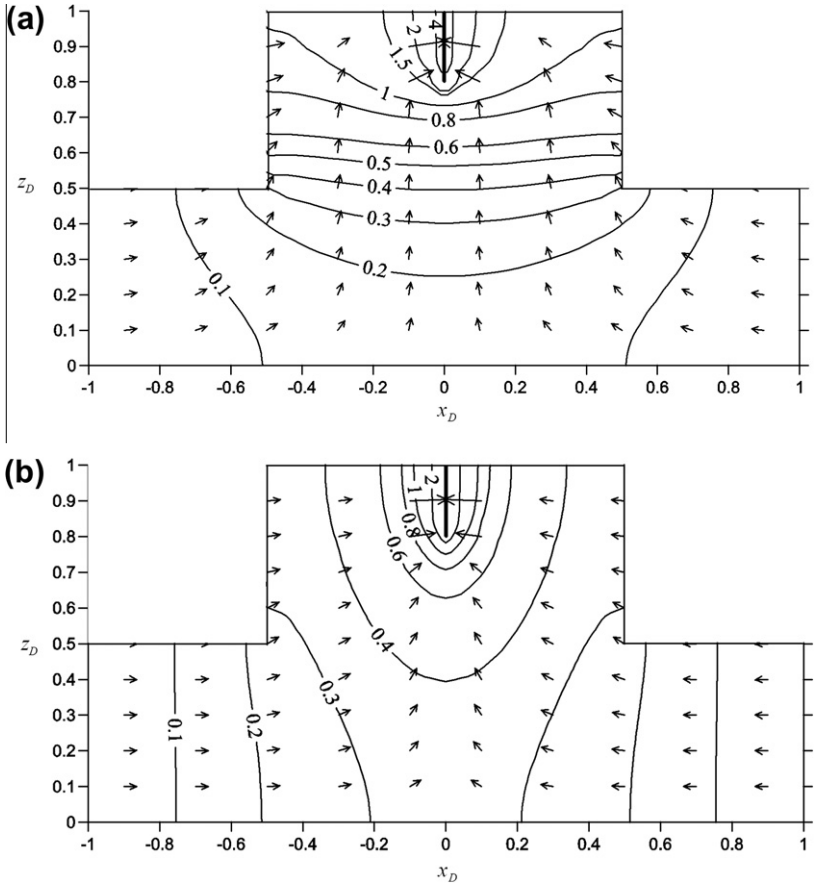


**Fig. 8.** Plots of dimensionless drawdown contours and flow fields for pumping at a partially penetrating well in the aquifers with the anisotropy ratios of (a) $\chi_{zx} = 0.3$ and (b) $\chi_{zx} = 3$. The dimensionless screen length of the pumping well is 0.2.

apparent vertical flow cross this region. Because $k_x$ is greater than $k_z$ in this case ($\chi_{zx} = 0.3$), most of flow goes through the horizontal path surrounding the well, leading to the larger drawdown in the upper zone 1 (i.e., $0.8 \leqslant z_D < 1$). The resultant hydraulic gradient as well as the boundary restriction causes an obvious vertical flow below this zone. On the other hand, Fig. 8b represents an uncommon case of $k_z$ greater than $k_x$ ($\chi_{zx} = 3$). In this case, the vertical path for flow into the well is superior to the horizontal one, which results in the contours around the well look like half ellipses. The flow in the limbs is mainly horizontal. However, obviously vertical flow can be observed in the central zone 1 below the well ($z_D < 0.8$ and $|x_D| < 0.2$) and around the concave corner of the top boundary in the anticline.

*3.3.2. Effect of well location*

Fig. 9 illustrates the influence of well location on the flow pattern. The dimensionless screen length of the partially penetrating well is considered to be $z_{Dl} = 0.2$; additionally, the isotropic anticline aquifer has the same geometry as the base case. Figs. 9a and b display the dimensionless drawdown contours at $y_D = 0$ for the pumping at a partially penetrating well located at the top-middle and bottom-middle of the aquifer, respectively. The flow patterns on the profile are symmetric to the midline of the aquifer. Most of water flows horizontally in the limbs except in the zone near the concave corner of the top boundary. Obviously vertical flows occur upward and downward in the aquifer as shown in Figs. 9a and b, respectively, especially in the zone toward the extremity of the well. The present solution can simulate the dimensionless drawdown for an arbitrarily located pumping well in the ridge zone. In the case of Fig. 9c, the partially penetrating well with the dimensionless screen length of 0.2 is located at a dimensionless distance of 0.25 from the midline of the anticline aquifer. The figure shows an asymmetrical flow pattern affected by the well location and aquifer geometry. Considerable vertical flow appears in the ridge zone and in the right limb, where $x_D < 0.35$. In addition, among these three cases, the well located at the top-middle of the aquifer, as shown in Fig. 9a, has the largest dimensionless drawdown around the well.

## 4. Conclusions

A mathematical model has been developed for describing the steady-state flow caused by the constant-flux pumping in an anticline aquifer. The proposed model accounts for the flow in response to partially or fully penetrating wells of infinitesimal diameter and with uniform inflow flux along the well screen. The anticline aquifer is homogeneous, anisotropic and confined with a shape mimicked by three consecutive blocks. The integral transform techniques FT and FFCT are applied to develop the steady-state solutions in transform space. The coefficients in the solutions require solving a system of linear equations represented in a matrix form. Finally, the Fourier inversion is applied to obtain the drawdown solution in real space.

The present solution is applicable to simulate the flow in a slab-shaped aquifer or a hillslope aquifer by assuming that two or three successive blocks are of the same height. For a slab-shaped aquifer, the simulated drawdown responses based on the present solution are identical to those evaluated by the image-well method when the well is fully penetrating and the aquifer is homogeneous, iso-

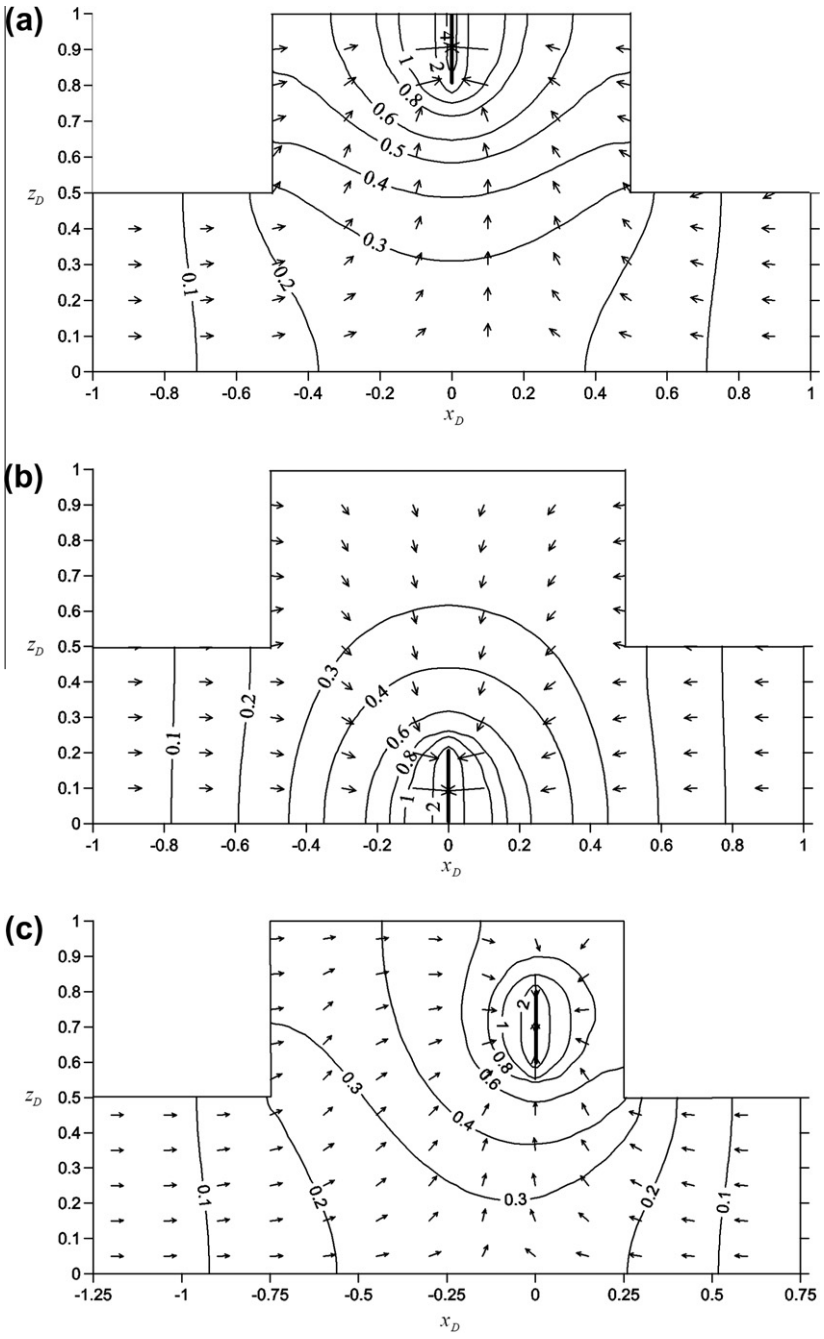


**Fig. 9.** Plots of dimensionless drawdown contours and flow fields for pumping at a partially penetrating well with the dimensionless screen length of 0.2. The wells are located at (a) $z_{0D}$ = 1.0 and (b) $z_{0D}$ = 0.2 on the midline of the anticline aquifer and (c) $z_{0D}$ = 0.8 at a dimensionless $x_D$ distance of 0.25 from the midline of the anticline aquifer.

tropic, confined and bounded by two parallel constant-head boundaries. Both the present solution and the numerical model, MODFLOW, are applied to simulate the case of flow in a hillslope aquifer. The grid settings allow MODFLOW to simulate the sloping boundary in a more realistic manner. Commonly, the dimensionless drawdown predicted by MODFLOW is slightly smaller than that by the present solution. In addition, the solution is used to investigate the influences of the aquifer geometry and anisotropy as well as the well partial penetration and location on the steady-state flow pattern. The results obtained from these cases exhibit significant vertical flow around the concave corner of the top boundary for a fully penetrating well or a partially penetrating well located at the hump zone of the anticline. The constant-flux pumping in a thin-limbs or narrow-ridged anticline would cause a much sharper head drop in the ridge zone. The influence of aquifer anisotropy on the observed drawdown cannot be ignored when the pumping is carried out in a partially penetrating well, especially for the well of short open screen. When the screen length or/and the anisotropy ratio decreases, the dimensionless drawdown around the pumping well increases under the same constant pumping rate. Finally, the present solution can simulate the flow field for an arbitrarily located pumping well. In inspecting the effect of well location, we find that the well located at the top-middle of the aquifer would produce larger drawdown around the well due to the boundary restriction on the anticline shape. The model MODFLOW, which can provide a better approximation on the curved boundary, is employed to simulate the flow field of the anticline aquifer. The simulated results are compared with

the predicted results from the present solution for flow toward a fully penetrating well in an anticline aquifer. MODFLOW gives slightly smaller dimensionless drawdown than the present solution in most regions, while the simulation is achieved by approximating the top boundary of aquifer with multiple steps. The drawdown solution developed in this study can be further applied to identify the aquifer parameters if integrated with an optimization algorithm and to perform preliminary assessment for the selection of a potential carbon sequestration site.


## Acknowledgements

The authors are grateful for support from Taiwan National Science Council under the Projects NSC99-2221-E-009-062-MY3, NSC98-3114-E-007-015, and NSC99-NU-E-009-001.


## Appendix A

The coefficients $V_0$, $V_n$, $W_0$ and $W_k$ in Eqs. (22), (26), (38), and (39) construct a system of $i+j+2$ linear equations, which can be expressed in matrix form as

$$\begin{bmatrix} 1+D_{00} & D_{01} & D_{02} & \dots & D_{0i} & E_{00} & E_{01} & E_{02} & \dots & E_{0j} \\ D_{10} & 1+D_{11} & D_{12} & \dots & D_{1i} & E_{10} & E_{11} & E_{12} & \dots & E_{1j} \\ D_{20} & D_{21} & 1+D_{22} & \dots & D_{2i} & E_{20} & E_{21} & E_{22} & \dots & E_{2j} \\ \vdots & \vdots & \vdots & \vdots & \vdots & \vdots & \vdots & \vdots & \dots & \vdots \\ D_{n0} & D_{n1} & D_{n2} & \dots & 1+D_{ni} & E_{n0} & E_{n1} & E_{n2} & \dots & E_{nj} \\ F_{00} & F_{01} & F_{02} & \dots & F_{0i} & 1+G_{00} & G_{01} & G_{02} & \dots & G_{0j} \\ F_{10} & F_{11} & F_{12} & \dots & F_{1i} & G_{10} & 1+G_{11} & G_{12} & \dots & G_{1j} \\ F_{20} & F_{21} & F_{22} & \dots & F_{2i} & G_{20} & G_{21} & 1+G_{22} & \dots & G_{2j} \\ \vdots & \vdots & \vdots & \vdots & \vdots & \vdots & \vdots & \vdots & \dots & \vdots \\ F_{k0} & F_{k1} & F_{k2} & \dots & F_{ki} & G_{k0} & G_{k1} & G_{k2} & \dots & 1+G_{kj} \end{bmatrix} \begin{bmatrix} V_0 \\ V_1 \\ V_2 \\ \vdots \\ V_i \\ W_0 \\ W_1 \\ W_2 \\ \vdots \\ W_j \end{bmatrix} = \begin{bmatrix} S_0 \\ S_1 \\ S_2 \\ \vdots \\ S_n \\ T_0 \\ T_1 \\ T_2 \\ \vdots \\ T_k \end{bmatrix} \tag{A1}$$

with the elements

$$D_{00} = z_{Db2}\alpha_0 C_{30}\left[\frac{1}{\gamma_0}C_{80} + \sum_{m=1}^{\infty}\frac{2\sin^2(\lambda_m z_{Db2})}{\gamma_m \lambda_m^2 z_{Db2}^2}C_{8m}\right] \tag{A2}$$

$$D_{0i} = \alpha_i C_{3i}\sum_{m=1}^{\infty}\frac{2\phi(m,i)\sin(\lambda_m z_{Db2})}{\gamma_m \lambda_m z_{Db2}}C_{8m} \tag{A3}$$

$$D_{n0} = \alpha_0 C_{30}\sum_{m=1}^{\infty}\frac{4\phi(m,n)\sin(\lambda_m z_{Db2})}{\gamma_m \lambda_m z_{Db2}}C_{8m} \tag{A4}$$

$$D_{ni} = \alpha_i C_{3i}\sum_{m=1}^{\infty}\frac{4\phi(m,n)\phi(m,i)}{\gamma_m z_{Db2}}C_{8m} \tag{A5}$$

$$E_{00} = -z_{Db3}\beta_0 C_{50}\left[\frac{1}{\gamma_0}C_{90} + \sum_{m=1}^{\infty}\frac{2\sin(\lambda_m z_{Db2})\sin(\lambda_m z_{Db3})}{\gamma_m \lambda_m^2 z_{Db2} z_{Db3}}C_{9m}\right] \tag{A6}$$

$$E_{0j} = -\beta_j C_{5j}\sum_{m=1}^{\infty}\frac{2\vartheta(m,j)\sin(\lambda_m z_{Db2})}{\gamma_m \lambda_m z_{Db2}}C_{9m} \tag{A7}$$

$$E_{n0} = -\beta_0 C_{50}\sum_{m=1}^{\infty}\frac{4\phi(m,n)\sin(\lambda_m z_{Db3})}{\gamma_m \lambda_m z_{Db2}}C_{9m} \tag{A8}$$

$$E_{nj} = -\sum_{j=1}^{\infty}\beta_j C_{5j}\sum_{m=1}^{\infty}\frac{4\phi(m,n)\vartheta(m,j)}{\gamma_m z_{Db2}}C_{9m} \tag{A9}$$

$$F_{00} = z_{Db2}\alpha_0 C_{30}\left[\frac{1}{\gamma_0}C_{90} + \sum_{m=1}^{\infty}\frac{2\sin(\lambda_m z_{Db2})\sin(\lambda_m z_{Db3})}{\gamma_m \lambda_m^2 z_{Db2} z_{Db3}}C_{9m}\right] \tag{A10}$$

$$F_{0i} = \alpha_i C_{3i}\sum_{m=1}^{\infty}\frac{2\phi(m,i)\sin(\lambda_m z_{Db3})}{\gamma_m \lambda_m z_{Db3}}C_{9m} \tag{A11}$$

$$F_{k0} = \alpha_0 C_{30}\sum_{m=1}^{\infty}\frac{4\vartheta(m,k)\sin(\lambda_m z_{Db2})}{\gamma_m \lambda_m z_{Db3}}C_{9m} \tag{A12}$$

$$F_{ki} = \alpha_i C_{3i}\sum_{m=1}^{\infty}\frac{4\vartheta(m,k)\phi(m,i)}{\gamma_m z_{Db3}}C_{9m} \tag{A13}$$

$$G_{00} = -z_{Db3}\beta_0 C_{50}\left[\frac{1}{\gamma_0}C_{80} + \sum_{m=1}^{\infty}\frac{2\sin^2(\lambda_m z_{Db3})}{\gamma_m \lambda_m^2 z_{Db3}^2}C_{8m}\right] \tag{A14}$$

$$G_{0j} = -\beta_j C_{5j}\sum_{m=1}^{\infty}\frac{2\vartheta(m,j)\sin(\lambda_m z_{Db3})}{\gamma_m \lambda_m z_{Db3}}C_{8m} \tag{A15}$$

$$G_{k0} = -\beta_0 C_{50}\sum_{m=1}^{\infty}\frac{4\vartheta(m,k)\sin(\lambda_m z_{Db3})}{\gamma_m \lambda_m z_{Db3}}C_{8m} \tag{A16}$$

$$G_{kj} = -\beta_j C_{5j}\sum_{m=1}^{\infty}\frac{4\vartheta(m,k)\vartheta(m,j)}{\gamma_m z_{Db3}}C_{8m} \tag{A17}$$

$$S_0 = \frac{q_D U_{c0}}{\gamma_0}C_{10}(x_{Da1P}) + \sum_{m=1}^{\infty}\frac{2q_D U_{cm}\sin(\lambda_m z_{Db2})}{\gamma_m \lambda_m z_{Db2}}C_{1m}(x_{Da1P}) \tag{A18}$$

$$S_n = \sum_{m=1}^{\infty}\frac{4q_D U_{cm}\phi(m,n)}{\gamma_m z_{Db2}}C_{1m}(x_{Da1P}) \tag{A19}$$

$$T_0 = \frac{q_D U_{c0}}{\gamma_0}C_{10}(x_{Da1N}) + \sum_{m=1}^{\infty}\frac{2q_D U_{cm}\sin(\lambda_m z_{Db3})}{\gamma_m \lambda_m z_{Db3}}C_{1m}(x_{Da1N}) \tag{A20}$$

and

$$T_k = \sum_{m=1}^{\infty}\frac{4q_D U_{cm}\vartheta(m,k)}{\gamma_m z_{Db3}}C_{1m}(x_{Da1N}) \tag{A21}$$

where

$$C_{8m} = \coth[\gamma_m(x_{Da1P} - x_{Da1N})], \quad m = 0,1,2,3,\dots \tag{A22}$$

and

$$C_{9m} = \operatorname{csch}[\gamma_m(x_{Da1P} - x_{Da1N})], \quad m = 0,1,2,3,\dots \tag{A23}$$

The subroutine DLSLRG of IMSL (2003) is used to solve Eq. (A1) by setting $i=j=k=n$ up to 100; accordingly, 202 linear equations should be solved simultaneously.

## References


Al-Mohannadi, N., Ozkan, E., Kazemi, H., 2007. Pressure-transient responses of horizontal and curved wells in anticlines and domes. SPE Reserv. Eval. Eng. 10 (1), 66–76.

Ashjari, J., Raeisi, E., 2006. Influences of anticlinal structure on regional flow, Zagros, Iran. J. Cave Karst Stud. 68 (3), 118–129.

Bergmann, P., Lengler, U., Schmidt-Hattenberger, C., Giese, R., Norden, B., 2010. Modelling the geoelectric and seismic reservoir response caused by carbon dioxide injection based on multiphase flow simulation: results from the $CO_2$ SINK project. Chem. Erde 70 (S3), 173–183.

Chan, Y.K., Mullineux, N., Reed, J.R., 1976. Analytical solutions for drawdowns in rectangular artesian aquifers. J. Hydrol. 31, 151–160.

Chan, Y.K., Mullineux, N., Reed, J.R., Wells, G.G., 1978. Analytic solutions for drawdowns in wedge-shaped artesian aquifers. J. Hydrol. 36, 233–246.

Chen, Y.J., Yeh, H.D., Yang, S.Y., 2009. Analytical solutions for constant-flux and constant-head tests at a finite-diameter well in a wedge-shaped aquifer. J. Hydraul. Eng. ASCE 135 (4), 333–337.

Connell, L.D., Jayatilaka, C., Bailey, M., 1998. A quasi-analytical solution for groundwater movement in hillslopes. J. Hydrol. 204 (1–4), 108–123.

Ferris, J.G., Knowles, D.B., Brown, R.H., Stallman, R.W., 1962. Theory of Aquifer Tests, Water-Supply Paper 1536-E, 104 p.

Förster, A., Norden, B., Zinck-Jørgensen, K., Frykman, P., Kulenkampff, J., Spangenberg, E., Erzinger, J., Zimmer, M., Kopp, J., Borm, G., Juhlin, C., Cosma, C., Hurter, S., 2006. Baseline characterization of the $CO_2$ SINK geological storage site at Ketzin, Germany. Environ. Geosci. 13 (3), 145–161.

IMSL, 2003. IMSL Fortran Library User's Guide Math/Library, vol. 2 of 2, Version 5.0, Visual Numerics, Houston, Texas.

Javandel, I., Zaghi, N., 1975. Analysis of flow to an extended fully penetrating well. Water Resour. Res. 11 (1), 159–164.

Jeffrey, A., Dai, H.H., 2008. Handbook of Mathematical Formulas and Integrals, fourth ed. Elsevier, 541 pp.

Kirkham, D., 1957. Potential and capacity of concentric coaxial capped cylinders. J. Appl. Phys. 28 (6), 724–731.

Kirkham, D., 1959. Exact theory of flow into a partially penetrating well. J. Geophys. Res. 64 (9), 1317–1327.

Streltsova, T.D., 1988. Well Testing in Heterogeneous Formations. John Wiley & Sons, New York, 413 pp.

Theis, C.V., 1935. The relation between the lowering of the piezometric surface and the rate and duration of discharge of a well using groundwater storage. Trans. Am. Geophys. Union 16 (1), 519–524.

Yeh, H.D., Chang, Y.C., 2006. New analytical solutions for groundwater flow in wedge-shaped aquifers with various topographic boundary conditions. Adv. Water Resour. 29 (3), 471–480.

Yeh, H.D., Kuo, C.C., 2010. An analytical solution for heterogeneous and anisotropic anticline reservoirs under well injection. Adv. Water Resour. 33 (4), 419–429.